Electronic Supplementary Material (ESI) for Physical Chemistry Chemical Physics.

Supplementary Information

Extending the Plasmonic Lifetime of Tip-enhanced Raman Spectroscopy Probes

Naresh Kumar[a,b*], Steve J. Spencer[a], Dario Imbraguglio[c], Andrea Rossi[c], Andrew J. Wain[a], Bert M. Weckhuysen[b], Debdulal Roy[a*]

[a] National Physical Laboratory, Hampton Road, Teddington, Middlesex TW11 0LW, UK
[b] Faculty of Science, Debye Institute for Nanomaterials Science, Utrecht University, Universiteitsweg 99, Utrecht 3584 CG, The Netherlands
[c] Istituto Nazionale di Ricerca Metrologica, Strada delle Cacce 91, 10135 Torino, Italy
* Email: naresh.kumar@npl.co.uk, debdulal.roy@npl.co.uk

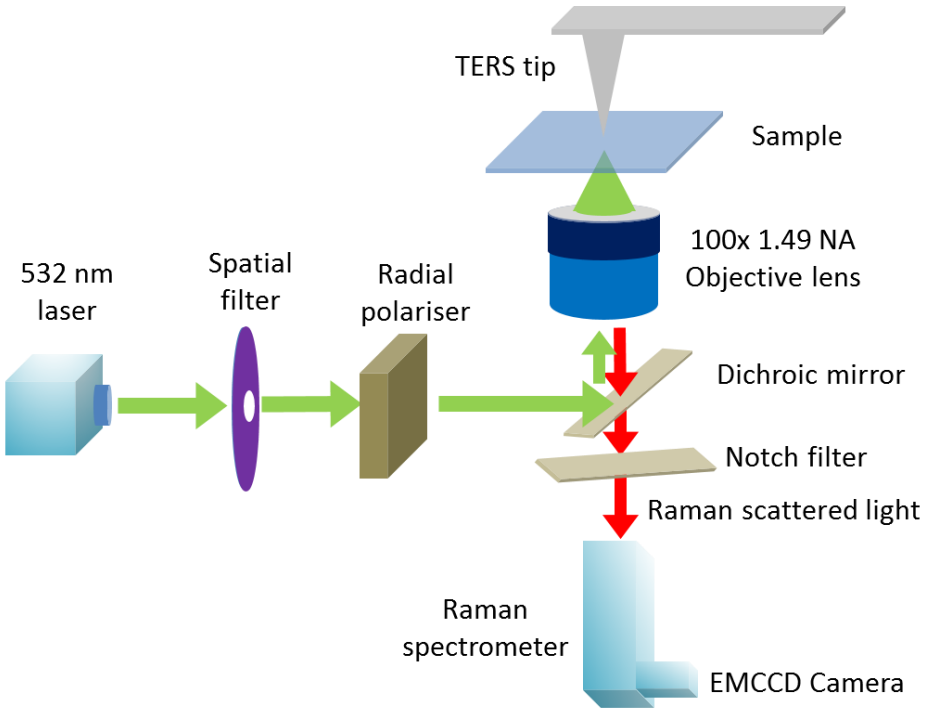

Fig. S1. Schematic diagram showing the detailed optical set-up of the bespoke TERS system used in this work.

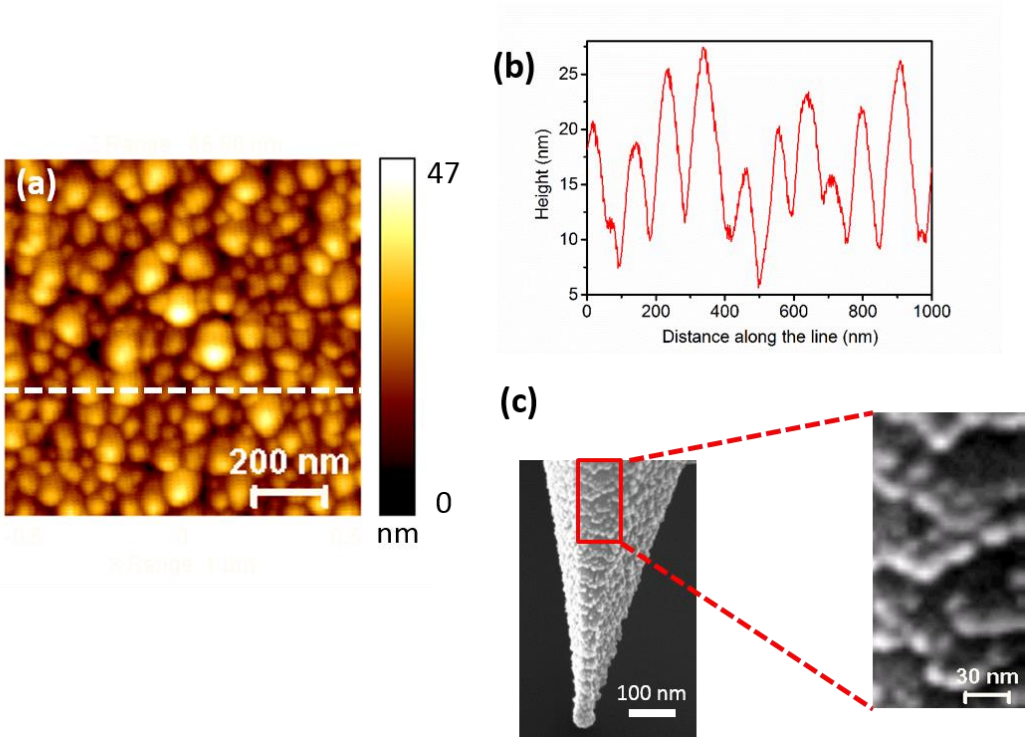

Fig. S2. (a) Topography image of Ag nanoparticles (NPs) on a Si substrate measured using tapping-mode AFM. (b) A representative height profile along the dashed line marked in (a). The height of the Ag NPs along the line ranges from 11 – 17 nm. (c) SEM image of a representative Ag-coated TERS tip shown in Figure 1. Zoomed in image of the area marked with red rectangle is shown in the inset. The Ag grains on the TERS tip are similar in size to the Ag NPs in (a).

Table S1. Binding energy of oxygen bonded to Ag, C and Si.

Oxygen bonding	**Binding energy (eV)**
AgO[1]	528.6
Ag_2O[1]	529.2
C=O[2]	531.3 – 532.4
C-O[2]	532.5 – 533.5
SiO_2[1]	532.5 – 534.3

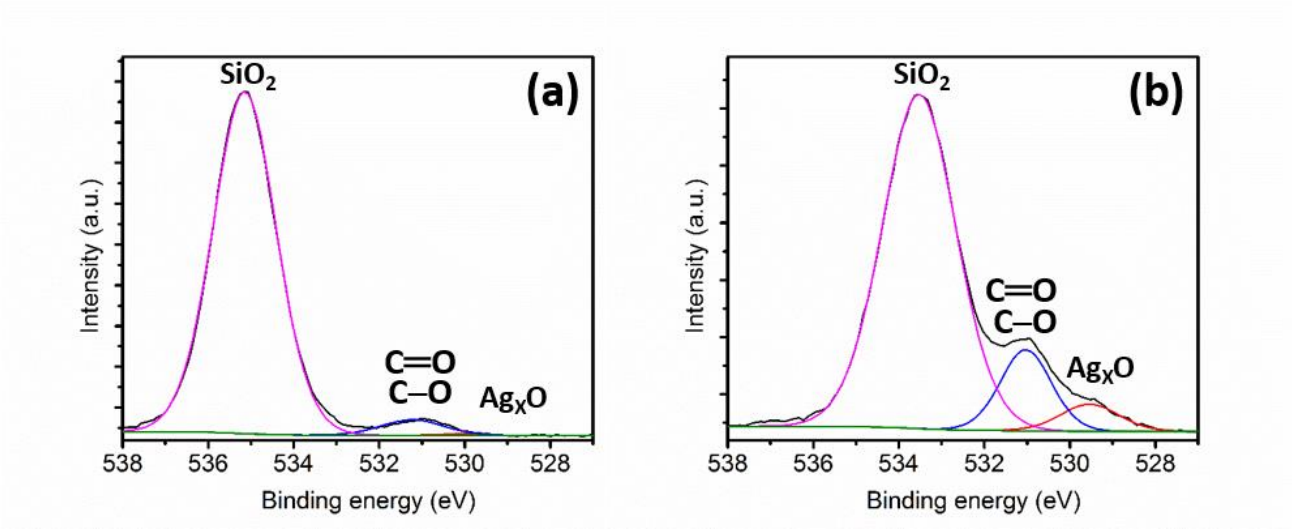

Fig. S3. O1s spectra of the Ag NPs after (a) 0 and (b) 17 h of exposure to the ambient environment. For the freshly prepared Ag NPs (0 h) a negligible amount of oxygen (0.1%) is bonded to Ag as shown (a). However, after 17 h of exposure to the ambient environment, the Ag NPs undergo surface oxidation increasing the atomic percentage of oxygen bonded to Ag from 0.1% to 2.1 %. The analysis of time-series XPS O1s spectra in Fig. S4a, 4b and S4b is explained in detail below:

The O 1s spectra have been fitted with 3 components: SiO_2, C bound to O and Ag_xO. It can be observed that the binding energy of the SiO_2 component shifts by -1.0 and -1.5 eV at 4 h and 17 h exposure respectively from its 0 h exposure position as shown in Table S2. However, the other components show no shift in binding energy over time. This suggests differential charging of SiO_2 on the sample surface is occurring during XPS measurements. Note that all spectra were acquired with the charge neutraliser switched on and were subsequently charge corrected by referencing to the C 1s hydrocarbon peak either from the same survey spectrum or from the relevant C 1s high resolution spectrum.

To confirm the differential charging of SiO_2 we looked at the binding energy of Si 2p peak in the XPS survey spectra and SiO2 peak in the O 1s spectra. As shown in Table S2 the SiO_2 component of the O 1s peak and the Si 2p peak in the survey spectrum show similar shifts in the time-series spectra, indicating that the component undergoing differential charging is correctly identified.

Table S2: Binding energy shifts of SiO_2 component of the O 1s peak and Si 2p peak in the survey spectra

Time	**Si 2p from survey spectra**		**SiO_2 component from O 1s Spectra**	
(Hours)	BE (eV)	Shift (eV)	BE (eV)	Shift (eV)
0	105.8	0.0	535.1	0.0
4	104.6	-1.2	534.1	-1.0
17	104.3	-1.5	533.5	-1.6

However, despite shift of SiO_2 peak due to differential charging, large binding energy difference between the SiO_2 and Ag_xO components in the O 1s spectra prevents a significant

overlap of their O 1s peaks. Therefore, the percentage of Ag_xO oxygen can be reliably calculated by careful fitting of O 1s spectra with three Gaussian-Lorentzian curves as shown in Fig. 4b of the main text and Supplementary Fig. S4b.

Table S3: Summary of time series XPS results on Ag NP samples with a thin and thick SiO_2 substrate

Time (Hours)	Sample 1 (Thin SiO_2)	Sample 2 (Thick SiO_2)
	Ag_XO atomic %	**Ag_XO atomic %**
0	0.0	0.18
17	5.17	3.58
	S atomic %	**S atomic %**
0	0.0	0.0
17	0.0	0.0

For further confirmation of the oxide formation on Ag NPs, XPS measurements were repeated at 0 and 17 hours on 2 more Ag NP samples with a thin (2 nm) and a thick (19 nm) layer of SiO_2 on Si substrate. Similar results of Ag_XO formation and absence of Sulphur were observed on both samples. A summary of the results is given in Table S3.

Supplementary Note 1

Principle of bilayer methodology

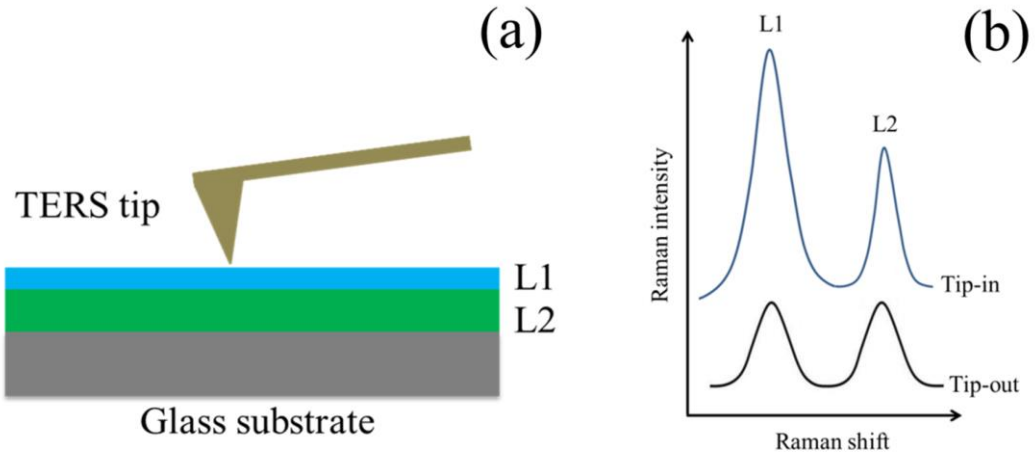

Fig. S4. (a) Schematic diagram of the bilayer sample showing the TERS tip, and the top and bottom layers, L1 (50 nm poly (3, 4 ethylenedioxythiophene):poly (styrenesulfonate) (PEDOT:PSS)) and L2 (350 nm polyacrylonitrile (PAN)), respectively. (b) Schematic spectra illustrating the principle of the bilayer methodology. In the "tip-in" Raman spectrum, only the Raman signals from the top layer L1 are plasmonically enhanced and the enhancement of the Raman signals from the bottom layer L2 occurs due to the increase in far-field signal arising from the reflections between the tip-shaft and the sample[3]. Raman signals from the bottom

layer has no near-field contribution because of the 50 nm thickness of the top layer, which is more than the decay length of the tip near-field (typically < 10 nm).

Calculation of TERS contrast[3]

The contrast of a near-field and far-field measurement on the bilayer is calculated through the following steps:

(a) First, the ratio of the far-field Raman intensities of two distinct peaks from top and bottom layers (K), when the tip is retracted from the sample is calculated:

$$K = \frac{I_{FF1}^{Tip-out}}{I_{FF2}^{Tip-out}} \tag{S1}$$

where $I_{FF1}^{Tip-out}$ and $I_{FF2}^{Tip-out}$ are the far-field Raman peak intensities from the unique and distinct peaks of the top and bottom layers, respectively.

(b) Then the ratio of the Raman intensities of two peaks from the top and bottom layers (R), when the tip is in contact with the bilayer sample, is calculated:

$$R = \frac{(I_{NF1}^{Tip-in} + I_{FF1}^{Tip-in})}{I_{FF2}^{Tip-in}} \tag{S2}$$

where, I_{NF1}^{Tip-in} and I_{FF1}^{Tip-in} are the near-field and far-field components of the Raman signal intensity of the top layer and I_{FF2}^{Tip-in} is the intensity of the Raman signal from the bottom layer, when the tip is in contact with the sample. Note that the Raman signal from the bottom layer does not have any near-field contribution in the tip-in spectrum.

(c) The factor by which the far-field intensity is increased when the tip is in contact with the sample (n), is calculated:

$$n = \frac{I_{FF2}^{Tip\text{-}in}}{I_{FF2}^{Tip\text{-}out}} = \frac{I_{FF1}^{Tip\text{-}in}}{I_{FF1}^{Tip\text{-}out}} \tag{S3}$$

(d) Finally, from Equations S1, S2 and S3 TERS contrast is calculated as:

$$contrast = \frac{I_{NF1}^{Tip\text{-}in}}{I_{FF1}^{Tip\text{-}out}} = n\left(\frac{R}{K} - 1\right) \tag{S4}$$

Equation S4 allows removal of the far-field contribution to the Raman signal of the top layer due to multiple reflections when the TERS tip is in contact with the sample, providing a more accurate estimation of the TERS contrast.

Supplementary Note 2

Further experimental details of XPS measurements

XPS survey spectra in the range 10 - 1300 eV binding energy were acquired at an emission angle of 0° to the surface normal. Analysis area was approximately 700 × 300 μm^2 with a sampling depth of < 10 nm. Analysis conditions used were 160 eV pass energy, 1 eV steps, 0.2 s dwell per step and 2 sweeps. High resolution O 1s spectra were also acquired using 40 eV pass energy, 0.1 eV steps, 0.5 s dwell per step and 2 sweeps. The charge neutraliser was used and charge correction later applied by referencing to the C 1s hydrocarbon peak at 285 eV, either in the survey spectra or from associated C 1s high-resolution spectra as appropriate. CasaXPS software was used to measure the peak areas of the survey spectra using a linear or Tougaard background as appropriate with the NPL transmission function (intensity) calibration[4] and average matrix relative sensitivity factors (AMRSF) to determine the concentrations of the detectable elements present.

Supplementary Note 3

Calculation of sampling depth of O1s electrons within Ag nanoparticles

A universal equation for the energy dependent effective electron attenuation length (*L*) for a material in X-ray photoelectron spectroscopy (XPS) is[5]

$$\lambda = \frac{0.65+0.007E^{0.93}}{Z^{0.38}} \quad \text{(S5)}$$

where, λ is the electron attenuation length in nm, *E* is the kinetic energy of O1s electrons (957.4 eV for Al monochromatic source) and *Z* is the average atomic number (47, 27.5 and 34 for Ag, AgO and Ag_2O, respectively). Using Equation (S5) λ for Ag, AgO and Ag_2O are measured to be 1.1, 1.4 and 1.3 nm, respectively.

The sampling depth (*S*) of XPS measurements, where 95% of the detected electrons come from, is represented by the equation[6]

$$S = 3 \times \lambda \quad \text{(S6)}$$

where, λ is the inelastic mean free path of O1s photoelectrons. From Equations (S5) and (S6) S is estimated to be 3.3, 4.2 and 3.9 nm for Ag, AgO and Ag_2O, respectively.

Supplementary Note 4

Chemical reactions of Ag with H_2O under ambient conditions

It has been observed that the presence of moisture on Ag surfaces plays a critical role in the atmospheric corrosion of Ag by providing a medium for the absorption of atmospheric gases and the dissolution of solid Ag. Furthermore, atmospheric carbon dioxide facilitates the corrosion of Ag by dissolving in the moisture layer on the Ag surface to form a weakly acidic solution. Hence, in the presence of moisture the corrosion of Ag proceeds according to the following chemical reactions[7]:
Oxidation of Ag:

$$Ag \rightarrow Ag^{+} + e^{-} \quad \text{(S7)}$$

This reaction is balanced in the acidic medium as:

$$O_2 + 4H_3O^{+} + 4e^{-} \rightarrow 6H_2O \quad \text{(S8)}$$

and

$$2H_3O^{+} + 2e^{-} \rightarrow 2H_2O + H_2 \quad \text{(S9)}$$

And in the neutral medium (although relatively uncommon for Ag under ambient conditions) as:

$$2H_2O + 2e^{-} \rightarrow H_2 + 2OH^{-} \quad \text{(S10)}$$

and

$$O_2 + 2H_2O + 4e^{-} \rightarrow 4OH^{-} \quad \text{(S11)}$$

Supplementary references

1. J. F. Moulder, W. F. Stickle, P. E. Sobol and K. D. Bomben "Handbook of X-ray Photoelectron Spectroscopy" Perkin-Elmer Corporation, USA ISBN: 0-9627026-2-5 (1992)
2. G. Beamson and D. Briggs "High Resolution XPS of Organic Polymers – The Scienta ESCA300 Database" John Wiley & Sons, UK ISBN: 0-47193592-1 (1992)
3. N. Kumar, A. Rae and D. Roy "Accurate measurement of enhancement factor in tip-enhanced Raman spectroscopy by elimination of far-field artefacts" Appl. Phys. Lett. **104**, 123106 (2014)
4. M. P. Seah "A System for the Intensity Calibration of Electron Spectrometers" *Journal of Electron Spectroscopy* **71,** 191-204 (1995)
5. M. P. Seah "Simple universal curve for the energy‐dependent electron attenuation length for all materials" *Surface and Interface Analysis*, **44(10)**, 1353-1359, (2012)
6. J. C. Vickerman and I. S. Gilmore "Surface Analysis – The Principal Techniques" 2nd Edition John Wiley & Sons, UK ISBN: 978-0-470-01763-0 (2009)
7. T. Graedel, "Corrosion Mechanisms for Silver Exposed to the Atmosphere" *Journal of the Electrochemical Society* **139**, 1963-1970 (1992)